AEDC-TDR-64-25

Schneider 1998

EQUATIONS AND CHARTS FOR THE EVALUATION OF THE HYPERSONIC AERODYNAMIC CHARACTERISTICS OF LIFTING CONFIGURATIONS BY THE NEWTONIAN THEORY

Approved for public release; distribution unlimited. } Per Gill Moss 10/7/98

By

E. L. Clark and L. L. Trimmer

von Kármán Gas Dynamics Facility
ARO, Inc.

TECHNICAL DOCUMENTARY REPORT NO. AEDC-TDR-64-25

March 1964

AFSC Program Element 65402034

(Prepared under Contract No. AF 40(600)-1000 by ARO, Inc., contract operator of AEDC, Arnold Air Force Station, Tenn.)

ARNOLD ENGINEERING DEVELOPMENT CENTER

AIR FORCE SYSTEMS COMMAND

UNITED STATES AIR FORCE

EQUATIONS AND CHARTS FOR THE EVALUATION OF THE HYPERSONIC AERODYNAMIC CHARACTERISTICS OF LIFTING CONFIGURATIONS BY THE NEWTONIAN THEORY

By

E. L. Clark and L. L. Trimmer
von Kármán Gas Dynamics Facility
ARO, Inc.
a subsidiary of Sverdrup and Parcel, Inc.

March 1964

ARO Project No. VT8002

AF - AEDC
Arnold AFS Tenn

ABSTRACT

The pressure distribution predicted by the modified Newtonian theory is used to develop equations for the aerodynamic forces, moments, and stability derivatives for components of hypersonic lifting configurations. In conjunction with the equations, a set of charts is presented to enable simple determination of the aerodynamic characteristics of swept cylinders, swept wedges, spherical segments, and cone frustums at zero sideslip and angles of attack from 0 to 180 deg. This method allows evaluation of most delta wing-body combinations without the need for numerical or graphical integration. As an example of the procedure, the theoretical characteristics of a blunt, 75-deg swept delta wing are calculated and compared with experimental results.

PUBLICATION REVIEW

This report has been reviewed and publication is approved.

Darreld K Calkins

Darreld K. Calkins
Major, USAF
AF Representative, VKF
DCS/Test

Jean A Jack

Jean A. Jack
Colonel, USAF
DCS/Test

CONTENTS

ILLUSTRATIONS

NOMENCLATURE

A	Body surface area
A_b	Base area of swept-wedge wing half
A_p	Planform area of swept-wedge wing half
A_s	Side area of swept-wedge wing half
b	Half-span of swept-wedge wing
C_A	Axial-force coefficient, $F_A/q_\infty S$
C_D	Drag coefficient, $\text{drag}/q_\infty S$
C_L	Lift coefficient, $\text{lift}/q_\infty S$
C_ℓ	Rolling-moment coefficient, $M_X/q_\infty S \ell$
C_{ℓ_β}	Rolling-moment coefficient derivative, $\partial C_\ell/\partial \beta$ at $\beta = 0$, 1/radian
C_m	Pitching-moment coefficient, $M_Y/q_\infty S \ell$
C_N	Normal-force coefficient, $F_N/q_\infty S$
C_n	Yawing-moment coefficient, $M_Z/q_\infty S \ell$
C_{n_β}	Yawing-moment coefficient derivative, $\partial C_n/\partial \beta$ at $\beta = 0$, 1/radian
C_p	Pressure coefficient, $(p - p_\infty)/q_\infty$
$C_{p_{max}}$	Pressure coefficient at stagnation point
$C_{p_{nose}}$	Pressure coefficient at nose of pointed body
C_Y	Side-force coefficient, $F_Y/q_\infty S$
C_{Y_β}	Side-force coefficient derivative, $\partial C_Y/\partial \beta$ at $\beta = 0$, 1/radian
c	Chord of swept-wedge wing
F	Function defining body surface
F_A	Axial force
F_N	Normal force
F_Y	Side force
h	Vertical displacement of swept-wedge wing half from wing centerline
$\bar{i}, \bar{j}, \bar{k}$	Unit vectors directed along the X-, Y-, and Z-axes, respectively

K	Proportionality constant used in the modified Newtonian theory
L	Body length
L_D	Delta-wing length, measured from theoretical apex
L/D	Lift-to-drag ratio
ℓ	Moment coefficient reference length
M_X	Rolling moment
M_Y	Pitching moment
M_Z	Yawing moment
M_∞	Free-stream Mach number
(n,x), (n,y), (n,z)	Angles between unit normal vector, $\bar{n}$, and the positive X-, Y-, and Z-axes, respectively
$\bar{n}$	Inward directed unit vector normal to the body surface
p	Surface static pressure
p_{t_2}	Stagnation pressure behind normal shock
p_∞	Free-stream static pressure
q_∞	Free-stream dynamic pressure
R	Radius of curvature
R_b	Base radius of cone frustum
R_n	Nose radius of cone frustum
r	Local body radius on cone frustum
S	Reference area
t	Thickness of swept-wedge wing half
V_∞	Free-stream velocity
X, Y, Z	Orthogonal body axes
X_T, Z_T	Moment transfer lengths
x, y, z	Coordinates along X-, Y-, and Z-axes
α	Angle of attack
α_o	Angle of attack where $\phi_o = -\phi'$ on swept-cylinder leading edge
α'	Angle between body X-axis and free-stream velocity vector

β	Angle of sideslip
Γ	Dihedral angle of swept-wedge wing
γ	Ratio of specific heats and wedge angle normal to leading edge of swept-wedge wing
δ	Half-angle of cone frustum and base tangent angle of spherical segment
δ_{nose}	Nose half-angle of pointed body
ϵ	Centerline angle of swept-wedge wing measured in X, Z- plane
η	Angle between surface unit inner normal vector and free-stream velocity vector
θ	Angular coordinate which defines cross-sectional planes
θ_b	Angle defining base location of spherical segment
Λ	Sweepback angle and base angle of spherical wedge
ξ	Cone frustum bluntness ratio, R_n/R_b
Φ	Angle of body roll measured in Y, Z- plane
ϕ	Angular coordinate which defines circumferential position in a cross-sectional plane
ϕ_o	Angle defining circumferential position where surface becomes shielded from the flow
ϕ'	Angle defining circumferential extent of swept-cylinder leading edge

SUBSCRIPTS

L	Lower half of swept-wedge wing
U	Upper half of swept-wedge wing

1.0 INTRODUCTION

In the design and testing of lifting re-entry configurations, there is often the need for a simple, approximate method of predicting the pressures and forces acting on the vehicle at hypersonic speeds. The Newtonian theory has proven very useful for this purpose. A number of studies have shown the accuracy of this simple theory in predicting the pressures and forces on such configurations as sharp and blunted cones (Refs. 1 through 5), circular cylinders (Refs. 6 and 7), hemispheres (Ref. 7), and delta wings (Ref. 8). Although the Newtonian theory is easily applied to the calculation of pressure distribution, integration of the pressure over the body surface to obtain total forces and moments can be difficult and time consuming. Hence, the theory is not always used to full advantage. Design charts which simplify the evaluation of body loads have been developed for complete and partial bodies of revolution (Refs. 5 and 9 through 13), elliptic cones (Refs. 5, 14, and 15), delta-wing components (Ref. 13), and three-dimensional bodies (Ref. 16). The charts of Refs. 5, 9, 11, 13, 14, and 15 provide total loads and derivatives for selected bodies, while the methods of Refs. 10, 12, and 16 apply to arbitrary bodies but require numerical or graphical integration.

The purpose of the present report is to extend the scope of the previous design charts by providing additional aerodynamic characteristics and an increased angle-of-attack range. To avoid a requirement of numerical integration, only selected configurations consisting of typical delta-wing and body components are considered. Equations are derived for the pressure distribution on each component, and this distribution is then integrated over the surface area in closed form to obtain total forces and moments. Equations and charts are given for the longitudinal stability and performance coefficients (C_N, C_A, C_m) and the directional and lateral stability derivatives $\left(C_{Y_\beta}, C_{n_\beta}, C_{\ell_\beta}\right)$ for an angle-of-attack range of 0 to 180 deg at zero sideslip.

An example of the use of the charts is given in the appendix, where the aerodynamic characteristics of a blunt, 75-deg swept delta wing are computed and compared with experimental results.

2.0 DEVELOPMENT OF EQUATIONS

The Newtonian theory has been discussed in a number of references, and only a brief summary will be given here. A thorough analysis of this theoretical method is given by Hayes and Probstein in Ref. 17.

Manuscript received January 1964.

Newton calculated the force on a body by assuming that the impact of fluid particles was completely inelastic for the normal component of momentum and was frictionless. Thus, the normal component of momentum is converted to a pressure force on the body while the tangential component remains unchanged. The analysis based on these assumptions gives the surface pressure coefficient, C_p, as

$$C_p = 2 \cos^2 \eta \tag{1}$$

where η is the angle between the free-stream velocity vector and the inward directed unit vector normal to the surface.

At high Mach numbers the disturbed region in front of a body becomes very limited in extent. The bow shock wave has approximately the same inclination as the body and is separated from the body surface by a very thin, practically inviscid, shock layer. With this flow geometry, the normal momentum of impinging molecules is lost inelastically and the tangential component of momentum is conserved. Hence, Newton's analysis is realistic for this type of flow, and the validity of the analysis increases as the shock-layer thickness decreases. For the shock wave to approach the inclination of the body, the gas dynamic equations show that the ratio of the density ahead of the shock to that behind the shock must approach zero. The equations further show that for the density ratio to approach zero, the Mach number must approach infinity and the ratio of specific heats must approach unity. If these Newtonian conditions ($M_\infty \to \infty$, $\gamma \to 1$) are satisfied, the Newtonian pressure coefficient, Eq. (1), is identical to that given by the oblique shock relations for the pressure immediately behind the shock wave.

In Newton's analysis, the impinging molecules leave the body surface along an unaccelerated path. However, in the case of a curved body with a thin shock layer, the particles are constrained in the shock layer and must follow an accelerated path. Therefore, for a correct analysis Eq. (1) must be modified to allow for the pressure gradient resulting from the centrifugal forces acting on the particles. This correction was first obtained by Busemann (Ref. 18), and the rational theory including the correction has been called the Newton-Busemann theory in Ref. 17. However, despite the theoretical correctness of the Newton-Busemann relation, the simple Newtonian theory has been found to agree much better with experimental data (e. g., Ref. 7), and the equations given in the present paper have not been corrected for centrifugal effects.

Equation (1) has been modified by a number of investigators to provide a better correlation with experimental data for several classes of bodies. The modified forms of the equation have the general relation,

$$C_p = K \cos^2 \eta \tag{2}$$

where K is a multiplicative factor which is used to match certain limiting conditions. For a flat plate with attached shock (i.e., at low angles of attack), Love (Ref. 19) suggested that $K = \gamma + 1$ provides better agreement with the exact oblique shock solution. For a slender pointed body with attached shock, best agreement with exact theory is obtained by using either the simple Newtonian value of $K = 2$ or the value suggested in Ref. 19 of $K = \frac{C_{p_{nose}}}{\sin^2 \delta_{nose}}$, where δ_{nose} is the surface angle at the nose and $C_{p_{nose}}$ is the exact value of pressure coefficient for this angle. Lees (Ref. 20) suggested that for a blunt body with detached shock wave the Newtonian theory could be modified to match conditions at the stagnation point by letting $K = C_{p_{max}} = \frac{p_{t_2} - p_\infty}{q_\infty}$, which is closely approximated by $K = \gamma + 3/\gamma + 1$ for large Mach numbers. In the present derivations, the modified form of the Newtonian approximation as given in Eq. (2) will be used with an arbitrary value of K.

The angle, η, between the velocity vector $\bar{V}_\infty$ and the surface unit inner normal vector $\bar{n}$ is determined by the scalar product of the two vectors. The velocity vector (Fig. 1) is

$$\bar{V}_\infty = -V_\infty \left(\bar{i} \cos\alpha \cos\beta + \bar{j} \sin\beta + \bar{k} \sin\alpha \cos\beta\right) \tag{3}$$

where $\bar{i}$, $\bar{j}$, and $\bar{k}$ are unit vectors directed along the X-, Y-, and Z-axes. The body surface may be described by the equation $F(x, y, z) = 0$. Then the inward directed unit vector normal to the body surface is

$$\bar{n} = \bar{i} \cos(n, x) + \bar{j} \cos(n, y) + \bar{k} \cos(n, z) \tag{4a}$$

where (n, x), (n, y), and (n, z) are the angles between $\bar{n}$ and the positive X-, Y-, and Z-axes, respectively, and their cosines are given by

$$\left.\begin{aligned} \cos(n, x) &= -\frac{\partial F / \partial x}{\sqrt{(\partial F/\partial x)^2 + (\partial F/\partial y)^2 + (\partial F/\partial z)^2}} \\ \cos(n, y) &= -\frac{\partial F / \partial y}{\sqrt{(\partial F/\partial x)^2 + (\partial F/\partial y)^2 + (\partial F/\partial z)^2}} \\ \cos(n, z) &= -\frac{\partial F / \partial z}{\sqrt{(\partial F/\partial x)^2 + (\partial F/\partial y)^2 + (\partial F/\partial z)^2}} \end{aligned}\right\} \tag{4b}$$

Thus,

$$\begin{aligned} \cos\eta &= \frac{\bar{V}_\infty \cdot \bar{n}}{V_\infty} \\ &= -\left[\cos\alpha \cos\beta \cos(n, x) + \sin\beta \cos(n, y) + \sin\alpha \cos\beta \cos(n, z)\right] \end{aligned} \tag{5}$$

The Newtonian theory predicts pressures only on surfaces which face the flow. For surfaces which are shielded from the flow, it is assumed that the surface pressure is equal to the free-stream static pressure and $C_p = 0$. Therefore, Eqs. (1) and (2) are applicable only for $\cos \eta \geq 0$.

Force and moment coefficient nomenclature utilized in the derivation is shown in Fig. 1. The coefficients are non-dimensionalized by an arbitrary reference area, S, and, in the case of moment coefficients, by an arbitrary reference length, ℓ. The moment reference point of each component is given in the corresponding figure. The coefficients are obtained by integrating the Newtonian pressure distribution over the body surface area, A, as indicated in the following general equations where the moment reference point is at the origin of the axes:

$$C_N = \frac{F_N}{q_\infty S} = -\frac{K}{S} \iint_A \cos^2 \eta \cos(n, z)\, dA \tag{6}$$

$$C_A = \frac{F_A}{q_\infty S} = -\frac{K}{S} \iint_A \cos^2 \eta \cos(n, x)\, dA \tag{7}$$

$$C_m = \frac{M_Y}{q_\infty S \ell} = -\frac{K}{S\ell} \left[\iint_A x \cos^2 \eta \cos(n, z)\, dA - \iint_A z \cos^2 \eta \cos(n, x)\, dA \right] \tag{8}$$

$$C_Y = \frac{F_Y}{q_\infty S} = \frac{K}{S} \iint_A \cos^2 \eta \cos(n, y)\, dA \tag{9}$$

$$C_n = \frac{M_Z}{q_\infty S \ell} = \frac{K}{S\ell} \left[\iint_A x \cos^2 \eta \cos(n, y)\, dA - \iint_A y \cos^2 \eta \cos(n, x)\, dA \right] \tag{10}$$

$$C_\ell = \frac{M_X}{q_\infty S \ell} = \frac{K}{S\ell} \left[\iint_A y \cos^2 \eta \cos(n, z)\, dA - \iint_A z \cos^2 \eta \cos(n, y)\, dA \right] \tag{11}$$

In the integration over the surface area, it is assumed that $C_p = 0$ on all surfaces shielded from the flow and on all flat surfaces (except in the case of the swept wedge) because these surfaces are usually concealed by other body components. Equations and charts are given for components having vertical symmetry and for the corresponding flat-topped components. For flat-bottomed components, the loads may be determined by taking the difference between the loads acting on the complete component and those acting on the flat-topped component and adding the pressure load of the flat lower surface to the normal force and pitching moment.

enough interest to warrant a presentation of the equations. Letting $\delta = 0$ in Eqs. (101), (108), and (112) gives, for $0 \leq \alpha \leq \pi$,

$$C_N \frac{S}{K R^2} = \frac{\pi}{4} \sin \alpha \, (1 + \cos \alpha) \tag{120}$$

$$C_A \frac{S}{K R^2} = \frac{\pi}{8} (1 + \cos \alpha)^2 \tag{121}$$

$$C_{Y_\beta} \frac{S}{K R^2} = - \frac{\pi}{4} (1 + \cos \alpha) \tag{122}$$

The moment coefficients and their derivatives are zero for a moment reference point at the center of curvature. The characteristics of the hemisphere are presented in Figs. 2 and 6.

2.2.4 Flat-Topped Hemisphere

For $0 \leq \alpha \leq \pi/2$ and $\delta = 0$, Eqs. (114), (115), and (119) give

$$C_N \frac{S}{K R^2} = \frac{\pi}{8} (1 + 2 \cos \alpha \sin \alpha + \sin^2 \alpha) \tag{123}$$

$$C_A \frac{S}{K R^2} = \frac{\pi}{8} (1 + 2 \cos \alpha \sin \alpha + \cos^2 \alpha) \tag{124}$$

$$C_{Y_\beta} \frac{S}{K R^2} = - \frac{\pi}{4} (\cos \alpha + \sin \alpha) \tag{125}$$

The moment coefficients and their derivatives are zero for a moment reference point at the center of curvature. For $\alpha \geq \pi/2$ the equations for the full hemisphere apply. The characteristics of the flat-topped hemisphere are presented in Figs. 3 and 7.

2.2.5 Cone Frustum

The cone frustum is frequently used as a nose or flare section of lifting bodies. The nomenclature used in the derivation is shown in Fig. J.

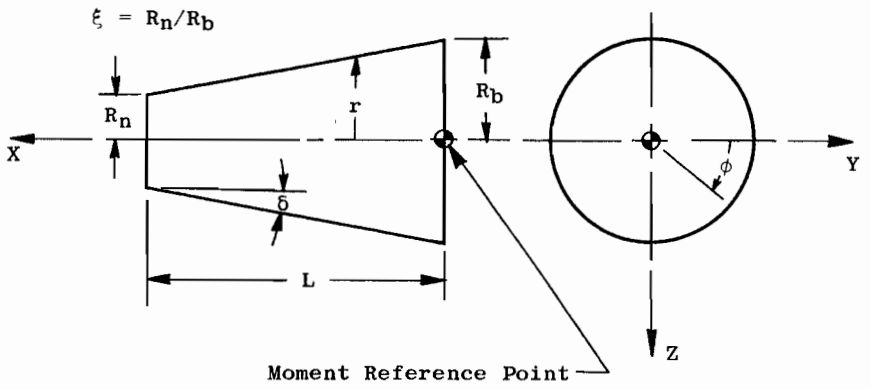

Fig. J Cone Frustum

The direction cosines of the inward directed unit normal vector are

$$\left.\begin{aligned} \cos(n,x) &= -\sin\delta \\ \cos(n,y) &= -\cos\delta\ \cos\phi \\ \cos(n,z) &= -\cos\delta\ \sin\phi \end{aligned}\right\} \tag{126}$$

Then, from Eq. (5)

$$\cos\eta = \cos\beta\ (\cos\alpha\ \sin\delta + \sin\alpha\ \cos\delta\ \sin\phi) + \sin\beta\ \cos\delta\ \cos\phi \tag{127}$$

At $\beta = 0$ the surface becomes shielded from the flow along a line defined by $\phi = \phi_o$, where

$$\phi_o = -\sin^{-1}\left(\frac{\tan\delta}{\tan\alpha}\right) \tag{128}$$

This equation is valid only for $\alpha \geq \delta$, since there is no shielding of the surface for $\alpha \leq \delta$. The elemental surface area is

$$dA = \frac{r\ d\phi\ dr}{\sin\delta} \tag{129}$$

It is assumed that $C_p = 0$ on the flat surfaces, and the coefficients and their derivatives are evaluated at $\beta = 0$.

2.2.5.1 Normal-Force Coefficient

The normal-force coefficient is given by

$$C_N = \frac{K}{S\tan\delta}\int_{\phi}\int_{R_n}^{R_b} r\cos^2\eta\ \sin\phi\ dr\ d\phi \tag{130}$$

Since ϕ_o is not a function of r, the first integral may be evaluated to give

$$C_N = \frac{K L R_b\ (1+\xi)}{2S}\int_{\phi}\cos^2\eta\ \sin\phi\ d\phi \tag{131}$$

where $\xi = R_n/R_b$.

Because of the limitations on the shielding equation, the integration of Eq. (131) must be treated as two separate cases. In each case, the integration is taken over the right side of the body and the result is multiplied by 2.

(I) $0 \leq \alpha \leq \delta$

$$C_N = \frac{K L R_b\ (1+\xi)}{S}\int_{-\pi/2}^{\pi/2}\cos^2\eta\ \sin\phi\ d\phi \tag{132}$$

which gives

$$C_N\ \frac{S}{K L R_b\ (1+\xi)} = \pi\ \cos\alpha\ \sin\alpha\ \sin\delta\ \cos\delta \tag{133}$$

(II) $\delta \leq \alpha \leq (\pi - \delta)$

$$C_N = \frac{K L R_b (1+\xi)}{S} \int_{\phi_o}^{\pi/2} \cos^2 \eta \sin \phi \, d\phi \tag{134}$$

which gives

$$C_N \frac{S}{K L R_b (1+\xi)} = \cos \alpha \sin \alpha \sin \delta \cos \delta \left[\frac{\pi}{2} + \sin^{-1} \left(\frac{\tan \delta}{\tan \alpha} \right) \right] + \left(\frac{2 \sin^2 \alpha \cos^2 \delta + \sin^2 \delta \cos^2 \alpha}{3 \sin \alpha \cos \delta} \right) \sqrt{\sin^2 \alpha - \sin^2 \delta} \tag{135}$$

At $(\pi - \delta) \leq \alpha \leq \pi$, $C_N = 0$. Equations (133) and (135) were evaluated for $\alpha = 0$ to 180 deg and $\delta = 0$ to 40 deg, and the results are presented in Fig. 8a.

2.2.5.2 Axial-Force Coefficient

The axial-force coefficient is given by

$$C_A = \frac{K}{S} \int_{\phi} \int_{R_n}^{R_b} r \cos^2 \eta \, dr \, d\phi \tag{136}$$

Integrating over r,

$$C_A = \frac{K L R_b (1+\xi)}{2 S} \tan \delta \int_{\phi} \cos^2 \eta \, d\phi \tag{137}$$

Evaluating Eq. (137) for the two cases:

(I) $0 \leq \alpha \leq \delta$

$$C_A = \frac{K L R_b (1+\xi)}{S} \tan \delta \int_{-\pi/2}^{\pi/2} \cos^2 \eta \, d\phi \tag{138}$$

which gives

$$C_A \frac{S}{K L R_b (1+\xi)} = \frac{\pi \tan \delta}{2} (2 \cos^2 \alpha \sin^2 \delta + \sin^2 \alpha \cos^2 \delta) \tag{139}$$

(II) $\delta \leq \alpha \leq (\pi - \delta)$

$$C_A = \frac{K L R_b (1+\xi)}{S} \tan \delta \int_{\phi_o}^{\pi/2} \cos^2 \eta \, d\phi \tag{140}$$

which gives

$$C_A \frac{S}{K L R_b (1+\xi)} = \frac{\tan \delta}{2} \left\{ (2 \cos^2 \alpha \sin^2 \delta + \sin^2 \alpha \cos^2 \delta) \left[\frac{\pi}{2} + \sin^{-1} \left(\frac{\tan \delta}{\tan \alpha} \right) \right] + 3 \cos \alpha \sin \delta \sqrt{\sin^2 \alpha - \sin^2 \delta} \right\} \tag{141}$$

At $(\pi - \delta) \leq \alpha \leq \pi$, $C_A = 0$. The numerical evaluation of Eqs. (139) and (141) are presented in Figs. 8b and c.

2.2.5.3 Pitching-Moment Coefficient

The pitching-moment coefficient is given by

$$C_m = \frac{K}{S\ell}\left[\int_\phi \int_{R_n}^{R_b} \frac{r(R_b - r)\cos^2\eta \sin\phi}{\tan^2\delta}\, dr\, d\phi - \int_\phi \int_{R_n}^{R_b} r^2 \cos^2\eta \sin\phi\, dr\, d\phi\right] \tag{142}$$

Integrating over r,

$$C_m = \frac{K}{S\ell}\left[\frac{1}{\tan^2\delta}\left(\frac{r^2 R_b}{2} - \frac{r^3}{3}\right) - \frac{r^3}{3}\right]_{R_n}^{R_b} \int_\phi \cos^2\eta \sin\phi\, d\phi \tag{143}$$

Substituting Eq. (131) into Eq. (143) gives

$$C_m = C_N \frac{R_b}{\ell \tan\delta}\left[1 - \frac{2}{3\cos^2\delta}\frac{(1-\xi^3)}{(1-\xi^2)}\right] \tag{144}$$

Since the limits of integration on ϕ do not enter into this derivation, Eq. (144) is valid for $0 \leq \alpha \leq \pi$.

2.2.5.4 Side-Force Coefficient Derivative

The side-force coefficient derivative is given by Eq. (112),

$$C_{Y_\beta} = -\frac{C_N}{\sin\alpha} \tag{145}$$

and C_{Y_β} may be obtained from Eqs. (133) and (135). For $\alpha = 0$, substituting Eq. (133) into Eq. (145) gives

$$\left(C_{Y_\beta}\right)_{\alpha=0} \frac{S}{KLR_b(1+\xi)} = -\pi \sin\delta \cos\delta \tag{146}$$

The numerical evaluation of Eqs. (145) and (146) is presented in Fig. 8d.

2.2.5.5 Yawing-Moment Coefficient Derivative

It is obvious from Eq. (145) that a general relation for all bodies of revolution is

$$C_{n_\beta} = -\frac{C_m}{\sin\alpha} \tag{147}$$

Substituting Eqs. (144) and (145) in Eq. (147) gives

$$C_{n_\beta} = C_{Y_\beta} \frac{R_b}{\ell \tan \delta} \left[1 - \frac{2}{3 \cos^2 \delta} \frac{(1 - \xi^3)}{(1 - \xi^2)} \right] \tag{148}$$

Like Eq. (144), this equation is valid for $0 \leq \alpha \leq \pi$.

2.2.5.6 Rolling-Moment Coefficient Derivative

The resultant force acts through the center of the cone, and there is no rolling moment about the indicated reference point. Therefore, $C_{\ell_\beta} = 0$.

2.2.6 Flat-Topped Cone Frustum

The geometry of the flat-topped cone frustum is shown in Fig. K.

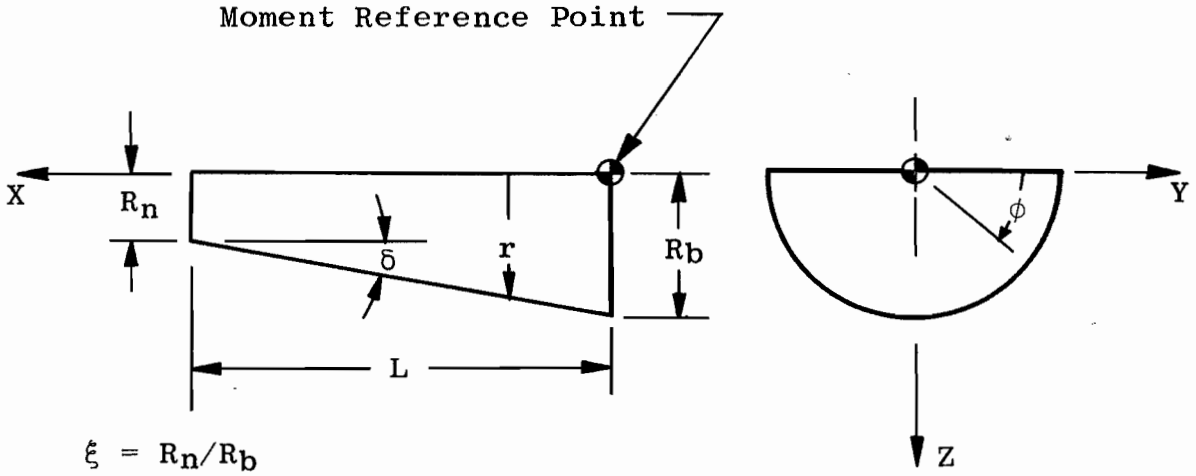

Fig. K Flat-Topped Cone Frustum

The direction cosines, pressure coefficient, and elemental area are the same as for the complete cone frustum. For $0 \leq \alpha \leq \pi/2$, the limits of integration on ϕ are from 0 to $\pi/2$. Then, from Eq. (131) and (137)

$$C_N \frac{S}{K L R_b (1 + \xi)} = \frac{\pi}{2} \cos \alpha \sin \alpha \sin \delta \cos \delta + \cos^2 \alpha \sin^2 \delta + \frac{2}{3} \sin^2 \alpha \cos^2 \delta \tag{149}$$

and

$$C_A \frac{S}{K L R_b (1 + \xi)} = \tan \delta \left[2 \cos \alpha \sin \alpha \sin \delta \cos \delta + \frac{\pi}{2} \left(\cos^2 \alpha \sin^2 \delta + \frac{\sin^2 \alpha \cos^2 \delta}{2} \right) \right] \tag{150}$$

Equations (145) and (146) apply only to the complete cone frustum, and C_{Y_β} for the flat-topped cone frustum must be obtained from Eq. (9).

REFERENCES

1. Penland, Jim A. "Aerodynamic Force Characteristics of a Series of Lifting Cone and Cone-Cylinder Configurations at a Mach Number of 6.83 and Angles of Attack up to 130°." NASA TN D-840, June 1961.

2. Ladson, Charles L. and Blackstock, Thomas A. "Air-Helium Simulation of the Aerodynamic Force Coefficients of Cones at Hypersonic Speeds." NASA TN D-1473, October 1962.

3. Neal, Luther, Jr. "Aerodynamic Characteristics at a Mach Number of 6.77 of a 9° Cone Configuration, with and without Spherical Afterbodies, at Angles of Attack up to 180° with Various Degrees of Nose Blunting." NASA TN D-1606, March 1963.

4. Fohrman, Melvin J. "Static Aerodynamic Characteristics of a Short Blunt 10° Semivertex Angle Cone at a Mach Number of 15 in Helium." NASA TN D-1648, February 1963.

5. Wells, William R. and Armstrong, William O. "Tables of Aerodynamic Coefficients Obtained from Developed Newtonian Expressions for Complete and Partial Conic and Spheric Bodies at Combined Angles of Attack and Sideslip with Some Comparisons with Hypersonic Experimental Data." NASA TR R-127, 1962.

6. Penland, Jim A. "Aerodynamic Characteristics of a Circular Cylinder at Mach Number 6.86 and Angles of Attack up to 90°." NACA TN 3861, January 1957.

7. Julius, Jerome D. "Experimental Pressure Distributions over Blunt Two- and Three-Dimensional Bodies Having Similar Cross Sections at a Mach Number of 4.95." NASA TN D-157, September 1959.

8. Bertram, Mitchel H. and Henderson, Arthur, Jr. "Recent Hypersonic Studies of Wings and Bodies." ARS Journal, Vol. 31, No. 8, August 1961, pp. 1129-1139.

9. Fisher, Lewis R. "Equations and Charts for Determining the Hypersonic Stability Derivatives of Combinations of Cone Frustums Computed by the Newtonian Impact Theory." NASA TN D-149, November 1959.

10. Rainey, Robert W. "Working Charts for Rapid Prediction of Force and Pressure Coefficients on Arbitrary Bodies of Revolution by Use of Newtonian Concepts." NASA TN D-176, December 1959.

11. Gray, J. Don. "Drag and Stability Derivatives of Missile Components According to the Modified Newtonian Theory." AEDC-TN-60-191, November 1960.

12. Margolis, Kenneth. "Theoretical Evaluation of the Pressures, Forces, and Moments at Hypersonic Speeds Acting on Arbitrary Bodies of Revolution Undergoing Separate and Combined Angle-of-Attack and Pitching Motions." NASA TN D-652, June 1961.

13. Malvestuto, Frank S., Jr., Sullivan, Phillip J., Marcy, William L., et al. "Study to Determine Aerodynamic Characteristics on Hypersonic Re-Entry Configurations: Analytical Phase, Design Charts." WADD-TR-61-56, Part II, Vol. 2, August 1962.

14. McDevitt, John B. and Rakich, John V. "The Aerodynamic Characteristics of Several Thick Delta Wings at Mach Numbers to 6 and Angles of Attack to 50°." (Title Unclassified) NASA TM X-162, March 1960. (Confidential)

15. Seaman, D. J. and Dore, F. J. "Force and Pressure Coefficients of Elliptic Cones and Cylinders in Newtonian Flow." Consolidated Vultee Aircraft Corporation, San Diego, California, ZA-7-004, May 16, 1952.

16. Jackson, Charlie M., Jr. "A Semigraphical Method of Applying Impact Theory to an Arbitrary Body to Obtain the Hypersonic Aerodynamic Characteristics at Angle of Attack and Sideslip." NASA TN D-795, May 1961.

17. Hayes, Wallace D. and Probstein, Ronald F. Hypersonic Flow Theory. Academic Press, New York, 1959.

18. Busemann, A. "Flüssigkeits-und-Gasbewegung." Handwörterbuch der Naturwissenschaften, Vol. IV, 2nd Edition, pp. 276-277, Gustau Fischer, Jena, 1933.

19. Love, Eugene S., Henderson, Arthur, Jr., and Bertram, Mitchel H. "Some Aspects of Air-Helium Simulation and Hypersonic Approximations." NASA TN D-49, October 1959.

20. Lees, Lester. "Hypersonic Flow." Fifth International Aeronautical Conference (Los Angeles, California, June 20-23, 1955), Institute of the Aeronautical Sciences, pp. 241-276.

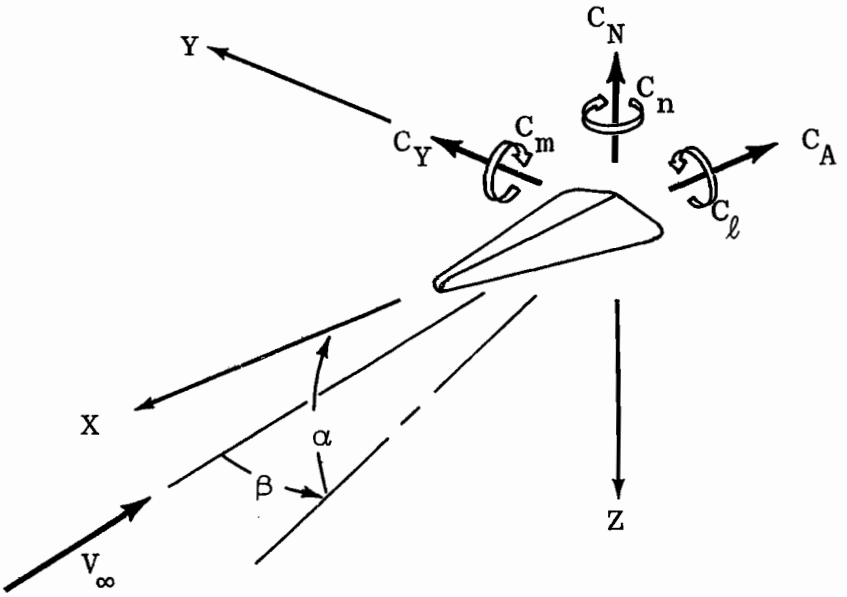

Fig. 1 Axis and Coefficient Nomenclature